



## Photo-oxidative degradation of toluene in aqueous media by hydroxyl radicals

Arzu Hatipoğlu<sup>a</sup>, Davide Vione<sup>b</sup>, Yelda Yalçın<sup>a</sup>, Claudio Minero<sup>b</sup>, Zekiye Çınar<sup>a,\*</sup>

<sup>a</sup> Yıldız Technical University, Department of Chemistry, 34220 Istanbul, Turkey

<sup>b</sup> Università di Torino, Dipartimento di Chimica Analitica, Via P. Giuria 5, 10125 Torino, Italy

### ARTICLE INFO

#### Article history:

Received 20 May 2010

Received in revised form 24 June 2010

Accepted 20 July 2010

Available online 29 July 2010

#### Keywords:

Toluene

Hydroxyl radical

Photo-oxidative degradation

DFT calculation

COSMO

### ABSTRACT

This study has the goal of determining the most probable reaction path and the product distribution for the photo-oxidative degradation of toluene in aqueous media. A combination of experimental and quantum mechanical methods were used to elucidate the effect of water solvent on the reaction rate and on the subsequent formation of the primary intermediates. In the experimental part of the study, the formation yields of hydroxylated intermediates and of benzaldehyde were measured by HPLC, in the presence of nitrate under UVB irradiation as the  $\bullet\text{OH}$  source. Modeling of the reaction paths was performed with density functional theory (DFT) calculations, to investigate the most plausible mechanism for the initial  $\bullet\text{OH}$  attack and to determine the identities of the primary intermediates. Rate coefficients for all the reaction paths were computed by the Transition State Theory (TST) to obtain the product distribution. The effect of solvent water was investigated by using COSMO as the solvation model. The experimental results combined with DFT calculations indicate that *ortho*-addition to finally give *o*-cresol is the dominant reaction path for gas and aqueous media. The presence of a dielectric medium such as water has a stabilizing effect that decreases the overall energy for this mechanism. Finally, the significance for surface waters of the reaction between toluene and  $\bullet\text{OH}$  was studied by use of a recently developed photochemical model that foresees the lifetime of a compound upon reaction with  $\bullet\text{OH}$ , as a function of the reaction rate constant, the chemical composition of the surface water layer, and the water column depth.

© 2010 Elsevier B.V. All rights reserved.

### 1. Introduction

Volatile aromatic compounds constitute an important class of water and air contaminants. They are mainly emitted into the environment from anthropogenic sources such as combustion processes, vehicle emissions and industrial sources, as well as from biogenic processes [1]. Recent calculations have shown that in urban areas up to 40% of photochemically produced ozone can be attributed to emissions of aromatics [2]. Furthermore, the degradation reactions of aromatic hydrocarbons yield non-volatile organic compounds that contribute to the formation of secondary organic aerosols [1]. The latter have serious effects on human health and the global climate [3]. The cited atmospheric reactions are also involved in the formation of polycyclic aromatic hydrocarbons, particulate matter and soot [4,5]. Therefore, the oxidative degradation mechanism of aromatic compounds is a current hot research topic.

Toluene is the most abundant volatile aromatic hydrocarbon present in the urban atmosphere, being a rather common constituent of crude oil and a major component of gasoline. It can

reach some 10 ppbv levels in polluted air [6] and even 1 ppmv in or near refueling stations [7]. The most important removal pathway of toluene from the atmosphere is the gas-phase reaction with  $\bullet\text{OH}$ , which mainly yields the hydroxylated derivatives (cresols) [1,8]. The latter are 7–11 times more reactive than toluene toward  $\bullet\text{OH}$  and, also being more water-soluble, can be more easily removed from the atmosphere [8].

Toluene is also present in surface and groundwater, usually because of fuel spills or petroleum production [9–15]. The concentration of toluene in surface waters is usually a fraction of  $\mu\text{g L}^{-1}$ , but values as high as  $\sim 10 \mu\text{g L}^{-1}$  have been described [14]. As a volatile organic compound, toluene can undergo partitioning between surface waters and the atmosphere, but additional processes are operational that account for its transformation [16], e.g. biodegradation [15]. Photochemistry is another important transformation route for water-dissolved pollutants [17], and the reaction with the hydroxyl radical ( $\bullet\text{OH}$ ) can play a key role in the photosensitized degradation of hardly oxidized aromatic compounds [18]. In recent years, advanced oxidation processes (AOPs) are being used in order to destroy toluene and other aromatic hydrocarbons in water or air. In all AOPs, including UV/ozone, UV/hydrogen peroxide and near-UV/titanium dioxide,  $\bullet\text{OH}$  radicals are generated by irradiation. These radicals initiate the degradation of all the aromatic hydrocarbons, but the transformation of pollu-

\* Corresponding author. Tel.: +90 212 383 4179; fax: +90 212 383 4134.

E-mail address: [cinarz@yildiz.edu.tr](mailto:cinarz@yildiz.edu.tr) (Z. Çınar).

tants may yield harmful intermediates that are more hazardous than the parent compounds. Therefore, knowledge on the intermediates and the reaction products is a necessity in the application of water and air treatment processes. Although the toluene +  $\bullet\text{OH}$  reaction has great importance in various fields of chemistry such as environmental chemistry, atmospheric chemistry and combustion chemistry, its degradation mechanism and product distribution is still uncertain.

The most important experimental result reported in the literature is that at room temperature the activation energy for the toluene +  $\bullet\text{OH}$  reaction is positive, whereas at high temperature it is negative [3]. The curved Arrhenius plots for this reaction have been attributed to the competition between different possible reaction paths. The reaction of toluene with  $\bullet\text{OH}$  radicals proceeds by three pathways: H-atom abstraction either from the side-chain or from the ring and addition to the aromatic ring. In the addition reactions, hydroxymethylcyclohexadienyl radical is formed. Of the hydroxylated adducts, *o*-cresol has been reported to be the most abundant [19]. On the other hand, in the H-abstraction paths from the methyl group and the ring, a benzyl and a methylphenyl radical are formed, respectively. The benzyl radical yields benzaldehyde through the reaction with  $\text{O}_2$ .

This paper has the purpose of determining the most probable reaction paths and the product distribution for the photo-oxidative degradation of toluene in aqueous media, to elucidate the effect of the water solvent on the reaction rate and on the subsequent formation of the primary intermediates. The experimental formation yields of the hydroxylated intermediates and of benzaldehyde were measured, and the most plausible reaction paths were modeled with density functional theory (DFT) calculations. These results were coupled with a recently developed photochemical model for surface waters, in order to assess the importance of the toluene +  $\bullet\text{OH}$  reaction in the aqueous environment [20,21].

## 2. Experimental details

### 2.1. Reagents and materials

Toluene (for residue analysis) was purchased from Fluka, benzaldehyde (>99.5%) and  $\text{H}_3\text{PO}_4$  (85%) from Aldrich, *o*-cresol (99%), *p*-cresol (99%) and benzoic acid (98%) from Carlo Erba, *m*-cresol (98%) and  $\text{NaNO}_3$  (99%) from Merck, acetonitrile (Supergradient grade) from Scharlau. All reagents were used as received, without further purification. Water used was of Milli-Q quality (>18  $\text{M}\Omega\text{ cm}^{-1}$ ,  $\text{TOC} \approx 2$  ppb).

### 2.2. Irradiation experiments

Solutions to be irradiated (5 mL total volume), containing 1 mM toluene and 0.1 M  $\text{NaNO}_3$  ( $\text{pH} \approx 6.5$ , measured with a Metrohm 713 pH meter equipped with a combined glass electrode), were placed into cylindrical Pyrex glass cells (4.0 cm diameter, 2.3 cm height). The solutions were magnetically stirred during irradiation, which was carried out under a 100 W Philips TL 01 lamp with emission maximum at 313 nm. The lamp had an irradiance of  $5.0 \pm 0.2 \text{ W m}^{-2}$ , measured with a CO.FO.ME.GRA. (Milan, Italy) power meter and corresponding to a photon flux of  $(3.3 \pm 0.1) \times 10^{-6} \text{ Einstein L}^{-1} \text{ s}^{-1}$  in the solutions, actinometrically determined with the ferrioxalate method [22]. Nitrate under UVB irradiation was used as the  $\bullet\text{OH}$  source to induce the transformation of toluene [23]; the lamp was chosen to achieve excitation of nitrate that has an absorption maximum at around 305 nm [17]. Fig. 1(a) reports the lamp emission spectrum, taken with an Ocean Optics SD 2000 CCD spectrophotometer and normalized to the actinometry data, also taking the transmittance of the Pyrex glass into

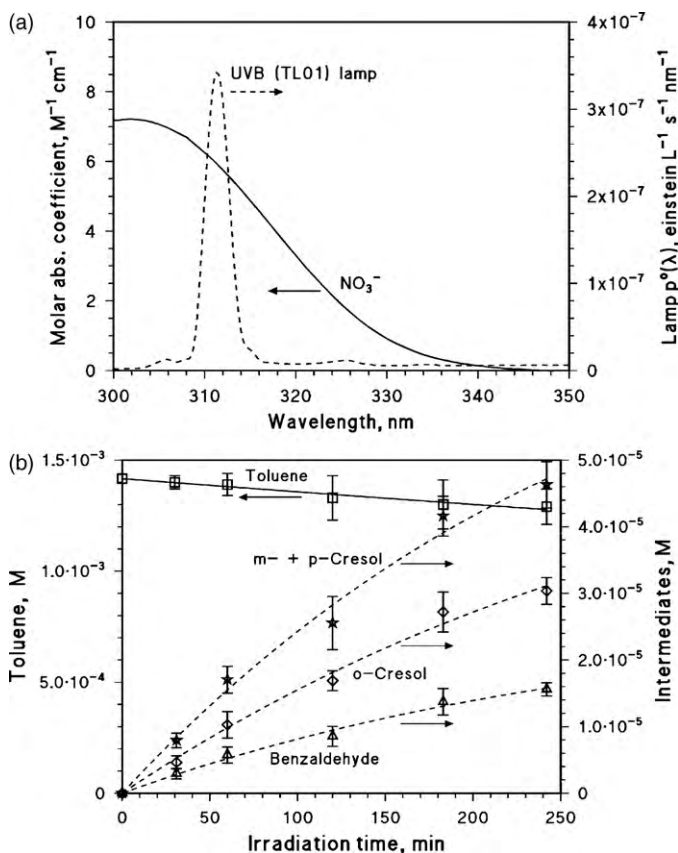


**Fig. 1.** (a) Emission spectrum of the UVB lamp (Philips TL 01) adopted for the irradiation experiments. Molar absorption coefficient of nitrate. (b) Time evolution of 1.4 mM toluene and of the detected transformation intermediates (cresols and benzaldehyde) upon UVB irradiation of 0.10 M  $\text{NaNO}_3$ ,  $\text{pH} \sim 6$ . The time evolution curve of toluene is plotted against the left-hand Y-axis, while those of the intermediates (cresols and benzaldehyde) are plotted against the right-hand Y-axis (note the different scales). The arrows point toward the axis relevant to each curve.

account. The Fig. also reports the absorption spectrum of nitrate, measured with a Varian Cary 100 Scan UV–vis spectrophotometer.

### 2.3. Analytical determinations

After irradiation, the solutions were analyzed with a Merck-Hitachi High-Pressure Liquid Chromatograph equipped with AS2000A autosampler, L-6200 and L-6000 pumps for high-pressure gradients, L-4200 UV–vis detector, and a RP-C18 LichroCART column (Merck, length 125 mm, diameter 4 mm) packed with LiChrospher 100 RP-18 ( $5 \mu\text{m}$  diameter). Elution was carried out with a 45:55 mixture of acetonitrile: aqueous  $\text{H}_3\text{PO}_4$  ( $\text{pH} 3$ ), at a flow rate of  $1.0 \text{ mL min}^{-1}$ . Injection volume was set at  $100 \mu\text{L}$ , detection wavelength at 210 nm. Under these conditions the retention times were (min): benzoic acid (2.60), *m*- and *p*-cresol (3.65), *o*-cresol (4.00), benzaldehyde (4.15), toluene (14.40). The column dead time was 0.90 min. The perfect co-elution of *m*- and *p*-cresol caused some problems, but they showed similar slopes in the calibration curve. For this reason, the sum of the concentrations of *m*- and *p*-cresol is reported in the parts that follow.

### 2.4. Kinetic data treatment

The concentration vs. time data of toluene and its transformation intermediates are the average results of a run carried out in triplicate. The time evolution data of toluene were fitted with Eq.

(1):

$$C_t = C_o \exp(-k_{tol}^d t) \quad (1)$$

where  $C_t$  is the concentration of toluene at the time  $t$ ,  $C_o$  its initial concentration, and  $k_{tol}^d$  the pseudo-first order degradation rate constant. The initial transformation rate of toluene is  $R_{tol} = k_{tol}^d C_o$ . The time evolution of each transformation intermediate was fitted with Eq. (2):

$$C_{int,t} = \frac{k_{int}^f C_o [\exp(-k_{tol}^d t) - \exp(-k_{int}^d t)]}{k_{int}^d - k_{tol}^d} \quad (2)$$

where  $C_o$ ,  $k_{tol}^d$  and  $t$  are as above,  $C_{int,t}$  is the concentration of the transformation intermediate at the time  $t$ , and  $k_{int}^f$ ,  $k_{int}^d$  are the pseudo-first order formation and transformation rate constants of the intermediate, respectively. The initial formation rate of each intermediate is  $R_{int} = k_{int}^f C_o$ , which is also the slope of the tangent to the relevant time evolution curve ( $C_{int,t}$  vs.  $t$ ) at  $t \rightarrow 0$ . The errors associated to the rates ( $\mu \pm \sigma$ ) represent the scatter of the experimental data around the fitting curve. The yields of the different intermediates were derived from the ratio of their initial rates to that of toluene, as  $\eta_{int} = R_{int} R_{tol}^{-1}$ . In the yield calculations we adopted the initial formation rates of the primary intermediates and of toluene ( $t \rightarrow 0$ ), because they are affected to a limited or negligible extent by the subsequent transformation of the intermediates by  $\bullet\text{OH}$  and/or direct photochemistry.

### 3. Computational set-up and methodology

#### 3.1. Computational models

The molecular models were created by using the mean bond distances, the geometric parameters of the benzene ring, tetrahedral angles for  $sp^3$ -hybridized carbon and oxygen atoms, and  $120^\circ$  for  $sp^2$ -hybridized carbon atoms. In the calculation of the hydroxylated radicals, the aromatic ring was left planar except for the position of attack. The attacking  $\bullet\text{OH}$  radical was assumed to form a tetrahedral angle with the C–H bond due to the change in the hybridization state of the carbon at the addition center from  $sp^2$  to  $sp^3$ .

#### 3.2. Methodology

The reaction system under consideration consists of  $\bullet\text{OH}$  radicals that are open-shell species. It is well-known that open-shell molecules pose severe problems in quantum mechanical calculations. Therefore, geometry optimization of the reactants, the product radicals, pre-reactive and transition state complexes were performed with the DFT method within the Gaussian 03 package [24]. DFT methods use the exact electron density to calculate molecular properties and energies, taking electron correlation into account. They do not suffer from spin contamination and this feature makes them suitable for calculations involving open-shell systems. The DFT calculations were carried out by the hybrid B3LYP functional, which combines HF and Becke exchange terms with the Lee–Yang–Parr correlation functional.

Choice of the basis set is very important in such calculations. In previous studies, radical addition reactions have been studied to determine the level of theory necessary for predicting energy barriers, and B3LYP/6-311+G(d,p)//B3LYP/6-31G(d) has been found to be the most suitable [25,26]. Based on these results, optimizations in the present study were performed at the B3LYP/6-31G(d) level followed by single point energy calculations at the B3LYP/6-311+G(d,p) level. The forming C–O bonds in the addition paths and the H–O bond in the abstraction path were chosen as the reaction coordinates in the determination of the transition states.

Ground-state and transition-state structures were confirmed by frequency analyses at the same level. Transition structures were characterized by having one imaginary frequency that belonged to the reaction coordinate, corresponding to a first-order saddle point. Zero-point vibrational energies (ZPEs) were calculated at the B3LYP/6-31G(d) level. The same ZPEs were used for the B3LYP/6-311+G(d,p)//B3LYP/6-31G(d) calculations. IRC calculations were performed for all of the transition geometries, and the corresponding maxima were confirmed.

#### 3.3. Solvent effect model

In aqueous media, water molecules affect the energetics of the degradation reactions of all organic compounds. Moreover,  $\text{H}_2\text{O}$  induces geometry relaxation on the solutes. The latter effect becomes more important when hydrogen-bonded complexes are present. However, the results obtained in earlier studies indicate that geometry changes have a negligible effect on the energy of the solute in water for both open- and closed-shell structures [27,28]. In this study, to take into account the effect of  $\text{H}_2\text{O}$  on the energetics and the kinetics of the toluene +  $\bullet\text{OH}$  reactions, DFT/B3LYP/6-311+G(d,p) calculations were carried out for the optimized structures of the reactants, the pre-reactive and the transition state complexes and the product radicals, by using COSMO (conductor-like screening solvation model) [28] as the solvation model, implemented in the Gaussian 03 package. The solvent was water at  $25^\circ\text{C}$ , with dielectric constant  $\epsilon = 78.39$  [29].

COSMO is one of the polarizable continuum methods (PCMs). In PCMs, the solute molecule is placed in a cavity surrounded by a polarizable continuum, whose reaction field modifies the energy and the properties of the solute [30]. The geometry of the cavity is determined by the shape of the solute. The reaction field is described in terms of apparent polarization charges or reaction field factors included in the solute Hamiltonian, so that it is possible to perform iterative procedures leading to the self-consistence between the solute wave-function and the solvent polarization. The COSMO method describes the solvent reaction field by means of apparent polarization charges distributed on the cavity surface, which are determined by imposing that the total electrostatic potential cancels out at the surface. This condition can describe the solvation in polar liquids. Hence, it is the method of choice in this study.

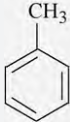
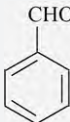
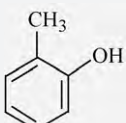
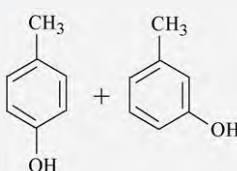
## 4. Results and discussion

#### 4.1. Photo-oxidation upon nitrate irradiation

Fig. 1(b) reports the time evolution of 1.4 mM toluene and of its identified transformation intermediates (*o*- and *m*- + *p*-cresol, benzaldehyde), upon UVB irradiation of 0.10 M  $\text{NaNO}_3$ . Interestingly, no formation of benzoic acid took place in the studied system at the adopted irradiation time scale (up to 4 h). The relevant values of  $R_{tol}$ ,  $R_{int}$  and  $\eta_{int}$  are presented in Table 1. Note that negligible direct phototransformation of toluene was observed in the absence of nitrate, under otherwise identical conditions.

Under the approximation of monochromatic irradiation that is reasonable for the 313-nm line of the adopted lamp, the photon flux absorbed by nitrate would be  $P_a^{\text{NO}_3^-} = P^\circ \times (1 - 10^{-A_{\text{NO}_3^-}})$ , where  $A_{\text{NO}_3^-} = \epsilon_{\text{NO}_3^-} b [\text{NO}_3^-]$ . At 313 nm (the lamp emission maximum in the UVB) it is  $\epsilon_{\text{NO}_3^-} = 5.7 \text{ M}^{-1} \text{ cm}^{-1}$ . It is also  $b = 0.40 \text{ cm}$ ,  $[\text{NO}_3^-] = 0.10 \text{ M}$  and  $P^\circ = (3.3 \pm 0.1) \times 10^{-6} \text{ Einstein L}^{-1} \text{ s}^{-1}$ . From these data one gets  $P_a^{\text{NO}_3^-} = 1.3 \times 10^{-6} \text{ Einstein L}^{-1} \text{ s}^{-1}$ . The observed degradation rate of toluene was  $R_{tol} = (9.85 \pm 0.79) \times 10^{-9} \text{ M s}^{-1}$  (see Table 1). A lower limit for the quantum yield of  $\bullet\text{OH}$  production

**Table 1**  
Initial degradation rate of 1.4 mM toluene and initial formation rates of the detected intermediates.

	Initial rate (M s <sup>-1</sup> )	Yields (%)
	$(9.85 \pm 0.79) \times 10^{-9}$	94.5 ± 19.4 <sup>a</sup>
	$(1.67 \pm 0.19) \times 10^{-9}$	17.0 ± 3.3
	$(3.00 \pm 0.35) \times 10^{-9}$	30.5 ± 6.0
	$(4.63 \pm 0.62) \times 10^{-9}$	47.0 ± 10.1

<sup>a</sup> The yield shown for toluene is the sum of the yields of the intermediates and of the associated errors.

upon nitrate photolysis,  $\phi_{\bullet\text{OH}}^{\text{NO}_3^-} = R_{\bullet\text{OH}}(P_a^{\text{NO}_3^-})^{-1} \geq R_{\text{tol}}(P_a^{\text{NO}_3^-})^{-1} = (7.3 \pm 0.6) \times 10^{-3}$ , can be obtained under the hypothesis that all photogenerated  $\bullet\text{OH}$  reacts with toluene. Such a result compares relatively well with the literature value  $\phi_{\bullet\text{OH}}^{\text{NO}_3^-} \approx 9 \times 10^{-3}$  [23].

All the detected intermediates are compatible with a reaction between toluene and  $\bullet\text{OH}$ . The radical would mainly attack the aromatic ring of toluene to produce the cresols (hydroxymethyl-benzenes) with a total yield of (78 ± 16)%, while benzaldehyde would derive from the attack of  $\bullet\text{OH}$  on the methyl group, with a yield of about 17 ± 3%. Evidence that  $\bullet\text{OH}$  is involved in the formation of benzaldehyde from toluene has been obtained both in the gas phase [8] and in aqueous solution [31].

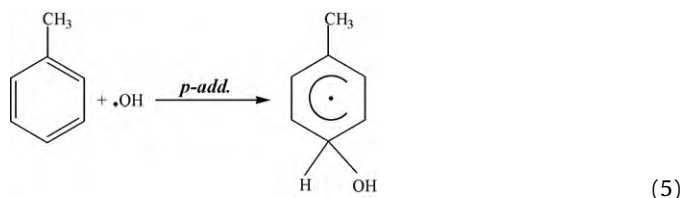
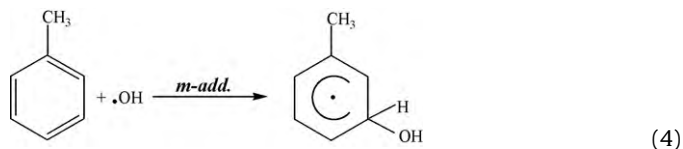
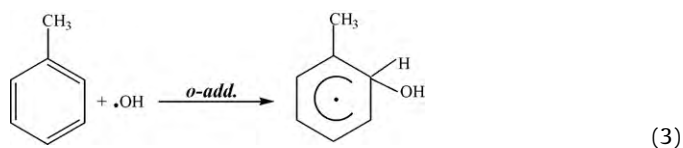
To make a comparison, in the gas phase the benzaldehyde yield from toluene +  $\bullet\text{OH}$  is reported to be 5–10%, while the cresols are formed in 20–30% yield (with *o*-cresol strongly prevailing over the *m*- and the *p*-isomers). Other intermediates detected in the gas phase include benzyl nitrate and *m*-nitrotoluene, but their formation would mainly be a consequence of the atmospherically relevant conditions chosen in the experiments (e.g. presence of  $\bullet\text{NO}$  and significant gas-phase nitration with  $\bullet\text{OH} + \bullet\text{NO}_2$ ) [8]. If only the common intermediates of the reactions in the gas phase and in water are considered, it can be seen that in both cases the  $\bullet\text{OH}$  attack on the ring prevails over that on the methyl group.

## 4.2. Computational modeling

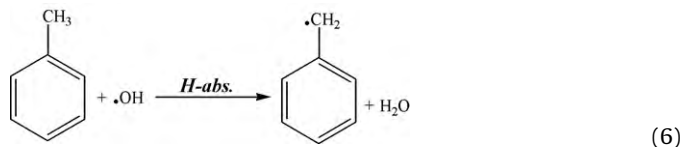
### 4.2.1. Reaction paths

The hydroxyl radical is a very active species and has a strong electrophilic character [32]. Once formed, it can readily attack the toluene molecule and produce the reaction intermediates.  $\bullet\text{OH}$  radical reactions with aromatic compounds proceed mainly by two reaction pathways: H-atom abstraction from C–H bonds and addition to aromatic rings [33]. Based on previous results [3,4,19], four different paths for the reaction of toluene with  $\bullet\text{OH}$  were deter-

mined. The first three paths, *ortho*-addition (*o*-add), *meta*-addition (*m*-add) and *para*-addition (*p*-add) to the ring are shown below:



The  $\bullet\text{OH}$  radical attacks a ring carbon with its unpaired electron and upon contact forms a C–O bond, while a  $\pi$ -bond of the aromatic system is broken and a hydroxymethylcyclohexadienyl radical is formed. The possibility of *ipso*-addition to the methyl-substituted site has been determined to be of minor importance [3]. The fourth reaction path:



consists in H-abstraction (H-abs) from the methyl group to produce a benzyl radical and a water molecule. The process of H-abstraction by the  $\bullet\text{OH}$  radical is a simple atom-transfer reaction in which the bond to the carbon atom in the –CH<sub>3</sub> group is broken and a new bond to the oxygen atom of the  $\bullet\text{OH}$  radical is formed. It has been suggested that ring abstraction paths are negligible at room temperature due to their larger energy barriers than side-chain abstraction paths [34,35].

### 4.2.2. Reactants and product radicals

Four different radicals were determined as the products of the reaction between toluene and the  $\bullet\text{OH}$  radical. The electronic and thermodynamic properties for the most stable conformers were also calculated. Fig. 2 represents the potential energy profile of the DFT-modeled mechanism for the initial attack of the  $\bullet\text{OH}$  radical to toluene.

The total energies for each of the reactants and the product radicals obtained for both gas and aqueous media (Fig. 2) indicate that the radicals, *o*-R, *m*-R and *p*-R produced in the addition paths are more stable than the H-R produced in the abstraction path. The reason may be attributed to the fact that all the radicals produced in the addition paths have hydrogen-bond-like stabilizations. The interaction distance between the original hydrogen atom at the addition center and the oxygen atom of the added  $\bullet\text{OH}$  was calculated to be 1.997 Å for *m*-R and *p*-R, while it is 1.999 Å for *o*-R. For the gas phase, among the three radicals produced in the addition paths, *o*-R has the lowest energy and is, therefore, the most stable one. The *p*-R is around 0.3 and *m*-R around 1.8 kcal mol<sup>-1</sup> less stable than *o*-R. The energy of H-R is too high to be compared with those of the addition radicals. For the aqueous phase, the sequence remains the same. The most and the least stable radicals are again the *o*-R and the H-R, respectively. However, all the product radi-



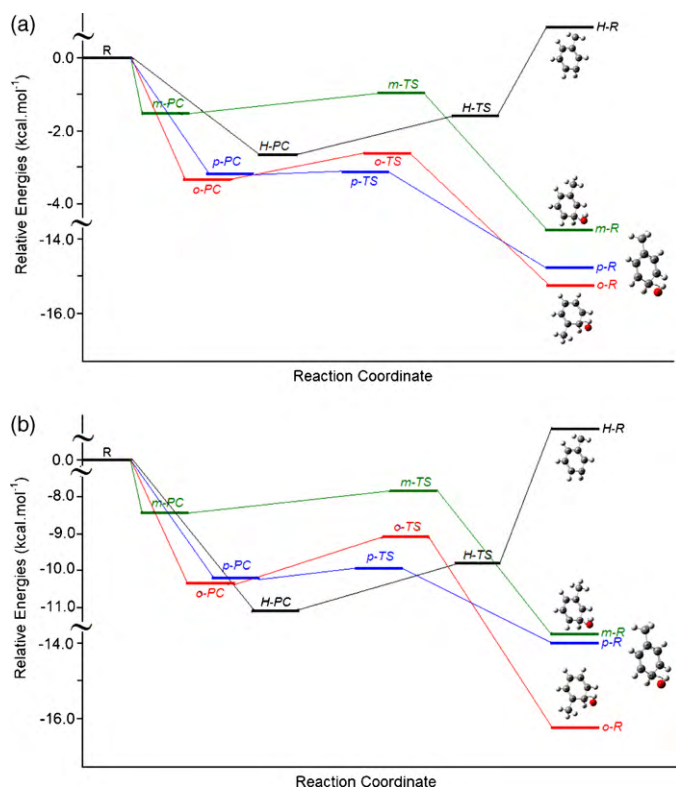


**Fig. 2.** (a) The potential energy profile of the DFT-modeled mechanism for the toluene +  $\bullet\text{OH}$  reaction in gas phase. (b) The potential energy profile of the DFT-modeled mechanism for the toluene +  $\bullet\text{OH}$  reaction in aqueous phase.

calcs are more stable in the aqueous phase, due to the newly formed hydrogen-bonds between their H atoms and the O atoms of the water molecules. The stabilities of the addition radicals increase by around  $8.6 \text{ kcal mol}^{-1}$  in the aqueous solution. On the other hand, the difference in the gas and aqueous-phase energies for H-R was much lower ( $4.2 \text{ kcal mol}^{-1}$ ). This is consistent with the fact that H-R has fewer hydrogen atoms, which causes weaker hydrogen-bonding compared to the hydroxylated adducts.

Adopting the localization approach of the Wheland's approximation [36], it may be predicted that  $\bullet\text{OH}$ -addition is the most probable reaction path and that the positions of attack of the  $\bullet\text{OH}$  radical are the *ortho* and *para* ones for both gas and aqueous phases. As seen in Fig. 2, the products of the three addition paths lie ca.  $15 \text{ kcal mol}^{-1}$  below the reactants. It may be concluded that the reactions will proceed to the corresponding products, once the reactants are sufficiently close to each other. The thermodynamically most favored product is 1-hydroxy-2-methylcyclohexadienyl radical, followed by 1-hydroxy-4-methylcyclohexadienyl radical for both gas and aqueous phases.

#### 4.2.3. Pre-reactive complexes

Our calculations indicated the formation of weakly bound complexes between the  $\bullet\text{OH}$  radical and toluene as the precursors of the reaction. Due to the existence of these pre-reactive van der Waals complexes, the reaction paths under investigation proceed over barriers that are lower in energy than the reactants. The pre-reactive complexes exert strong influence over the kinetics of the reactions by altering barrier heights and by affecting the energy partitioning of the reaction products. Furthermore, the presence of such complexes affects the reaction dynamics by spatially directing the site of the reaction, either by steric direction or by providing a low potential well that favors a reaction site.

Depending on the direction of approach of the  $\bullet\text{OH}$  radicals, four different chemically activated pre-reactive complexes, *o*-PC, *m*-PC, *p*-PC and H-PC with shallow wells, ca.  $3 \text{ kcal mol}^{-1}$  were determined for both gas and aqueous phases. The optimized structures of the pre-reactive complexes are shown in Fig. 3. The  $\bullet\text{OH}$  radical is seen to approach the aromatic ring from above, lying almost parallel to the ring plane with a deviation of about  $5\text{--}10^\circ$ . In the addition complexes, the hydrogen atom was found to be facing toward the center of the ring, while the ring carbons at the addition centers were found to deviate from the ring plane by around  $2^\circ$ . The main difference in the optimized geometries occurs in the distance between the oxygen atom of  $\bullet\text{OH}$  and the ring carbon. *m*-PC has much longer distance as compared with  $1.9 \text{ \AA}$  in *o*-PC and  $1.4 \text{ \AA}$  in *p*-PC. Energetically the *o*-PC and *p*-PC are the most stable complexes followed by H-PC, lying  $3.27$ ,  $3.22$  and  $2.95 \text{ kcal mol}^{-1}$  below the isolated reactants, respectively. The least stable pre-reactive complex is the *m*-PC, which is around  $1.39 \text{ kcal mol}^{-1}$  less stable than *o*-PC. It is observed that the stability of the pre-reactive complexes is higher in the aqueous than in the gas phase, because the presence of water molecules, hydrogen-bonded to the hydrogen atoms of the complexes lowers the total energies. The reduction in energy was calculated to be ca.  $6.65 \text{ kcal mol}^{-1}$  for the three addition complexes and ca.  $8.24 \text{ kcal mol}^{-1}$  for the H-PC. Although the energy gain of the reactants by complex formation is much less in water, the newly formed hydrogen-bonds between the complex and the water molecules make the structures more stable.

#### 4.2.4. Transition state complexes

Four transition state complexes *o*-TS, *m*-TS, *p*-TS and H-TS, one for each of the possible reaction paths were identified. The optimized structures of the TS are displayed in Fig. 4. In all the complexes the  $\bullet\text{OH}$  radical is almost parallel to the ring plane, with slight deviations of ca.  $0.5^\circ$  in *p*-TS and H-TS, and  $7^\circ$  in *o*-TS and *m*-TS. The oxygen atom points to the carbon atom at the reaction center, while the hydrogen atom points to the center of the aromatic ring. The hydrogen atom at the addition center rotates out of the ring plane to the opposite side of  $\bullet\text{OH}$ , by  $13.9^\circ$ ,  $15.5^\circ$  and  $3.3^\circ$  in *o*-TS, *m*-TS and *p*-TS, respectively.

In the addition paths the major structural changes in the ring geometry relative to the parent toluene molecule are all localized around the carbon atom at the reaction center. The two C–C bonds connecting the addition center lengthen by  $0.025\text{--}0.029 \text{ \AA}$ , whereas the change in the bond lengths of the subsequent bonds is lower, around  $0.005 \text{ \AA}$ . This finding indicates that the two C–C bonds connecting the addition center have single rather than double bond character. The bonds away from the addition center have a more pronounced double bond character. In the H-TS all the geometric changes are located around the methyl group and the carbon atom connecting it. Since a new bond is being formed between one of the hydrogen atoms of the methyl group and the oxygen atom of the  $\bullet\text{OH}$  radical, H–C–H angles in the methyl group become narrower by  $4^\circ$ . There is also a slight elongation in the breaking bond, around  $0.2 \text{ \AA}$ .

In the light of the potential energy profiles reported in Fig. 2, it may be suggested that the forming bond length is a sensitive measure of the formation of the transition state complex along the reaction coordinate. As displayed in Fig. 4, the addition complexes have much longer C–O bonds,  $2.062$ ,  $2.032$  and  $2.431 \text{ \AA}$  in *o*-TS, *m*-TS and *p*-TS, respectively, as compared to the C–O bonds in the corresponding radicals,  $1.45 \text{ \AA}$ . This suggests that the addition complexes are early transition states, whereas the abstraction complex is formed late along the reaction coordinate. Among the three addition complexes the longest C–O bond belongs to the *p*-TS, while the *m*-TS and *o*-TS have much shorter C–O bonds. This indicates that they are formed late as compared to *p*-TS and that, therefore, *p*-TS is the earliest transition state. Furthermore, the *p*-TS was found to

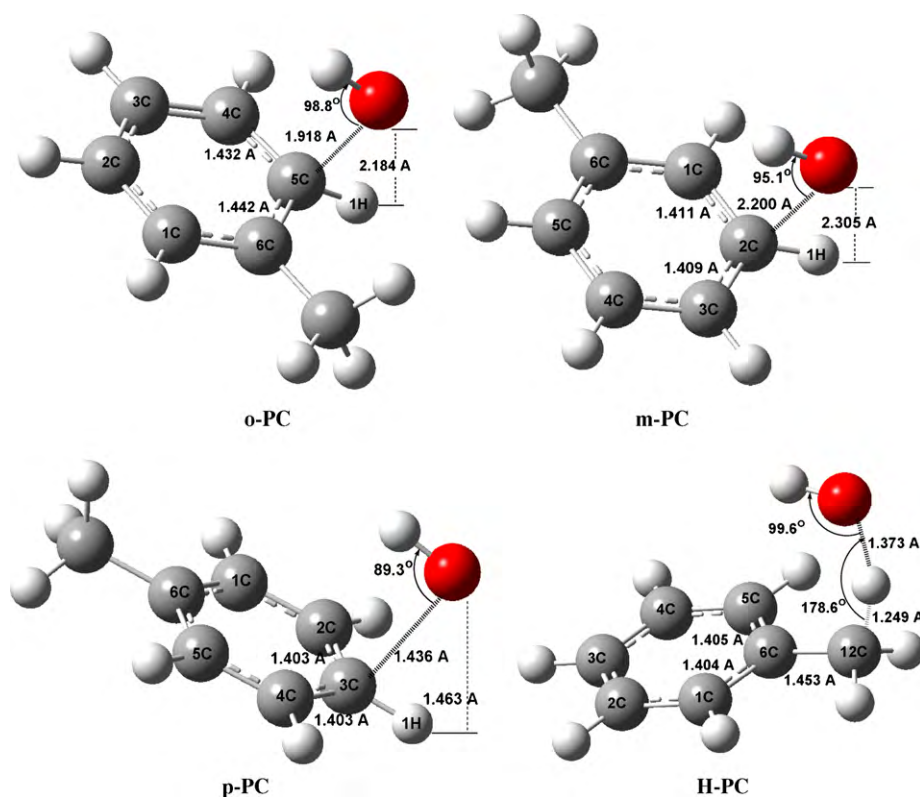


Fig. 3. The optimized structures of the pre-reactive complexes.

have the lowest total energy among all the possible transition states (Fig. 2), indicating that it is the most thermodynamically stable one. The transition-state structures, *p*-TS, *o*-TS, H-TS and *m*-TS lie 3.23, 2.89, 1.88 and 1.46 kcal mol<sup>-1</sup>, respectively, below the reactants. Thus, it may be concluded that in the photo-oxidative degradation of toluene, *p*-TS occurs early along the reaction coordinate, giving rise to a long C–O bond and a low total energy. As a consequence, it is the most probable transition-state structure. It was observed that the stability order changes in the aqueous phase, where the H-TS has lower energy than *o*-TS. However, the stability of all the transition-state structures increases due to weak interactions with the water molecules. Although the energies of all the transition state complexes decrease by around 7 kcal mol<sup>-1</sup>, the *p*-TS is the most thermodynamically stable TS for the aqueous phase as well.

#### 4.2.5. Energetics of the reaction paths

The activation energies  $E_a$  for the four possible reaction paths were calculated and presented in Table 2 along with the reaction energies  $\Delta E_r$ , for both gas and aqueous phases. The values in Table 2 show that the activation energies for the three •OH-addition paths are lower than for H-abstraction. The lowest activation energy in the gas phase belongs to the *para*-addition path. The energy barrier for the *ortho*-addition path is 0.37 kcal mol<sup>-1</sup> higher than for *para*-addition. In the aqueous phase, the stability order of the transition state complexes changes in favor of *ortho*-addition. Although water has a stabilizing effect in terms of total energies, the energy barriers in aqueous solution for the *para*- and *meta*-addition paths are slightly higher than the barriers in the gas phase. They increase by around 0.49 and 0.13 kcal mol<sup>-1</sup>, respectively, because of the prevention of the formation of the nice intramolecular hydrogen-bond network observed in the two transition state complexes. In contrast, the activation energy for the *ortho*-addition path decreases by around 0.12 kcal mol<sup>-1</sup>, causing the relevant reaction path to have the lowest activation energy among all the possible ones. In

the aqueous phase, the barrier for H-abstraction also decreases by ca. 0.06 kcal mol<sup>-1</sup>. The reason may be attributed to the additional stabilizing effect of the newly formed hydrogen-bonds with the water molecules. Moreover, *para*- and *ortho*-addition paths were found to have the highest exothermicities in the gas phase, whereas the *ortho*-addition path has the highest exothermicity in the aqueous phase. The result is consistent with Hammond's postulate [37], which states that early transition states have low energy barriers and high exothermicities. So, it may be concluded that *p*-TS and *o*-TS are the most probable transition states for gas and aqueous phases, respectively.

#### 4.2.6. Reaction rates and product distribution

The rate constant  $k$  for each reaction path was calculated by using the Transition State Theory for 300 K. The classical rate constant  $k$  in the Transition State Theory is given by Eq. (7):

$$k = \frac{k_B T}{h} \frac{q_{TS}}{q_T q_{OH}} e^{-E_a/RT} \quad (7)$$

where  $k_B$  is Boltzmann's constant,  $T$  is temperature,  $h$  is Planck's constant,  $q$ 's are molecular partition functions for TS and the reactant species, toluene and •OH, and  $E_a$  is the activation energy. Each of the molecular partition functions was assumed to be the product of translational, rotational, vibrational and electronic partition functions of the corresponding species.

The calculated rate constants in Table 2 show that in the gas phase the highest rate constant belongs to *para*-addition, followed by *ortho*- and *meta*-addition, whereas H-abstraction is the slowest reaction path, consistent with its high energy barrier. The branching ratio for each of the reaction paths was calculated by dividing the corresponding rate constant by the sum of the rate constants, taking the number of similar addition centers into account. The overall rate constant for the gas phase was calculated to be  $3.79 \times 10^{-13}$  cm<sup>3</sup> molecule<sup>-1</sup> s<sup>-1</sup> at 300 K which is in perfect agreement with the experimental value of

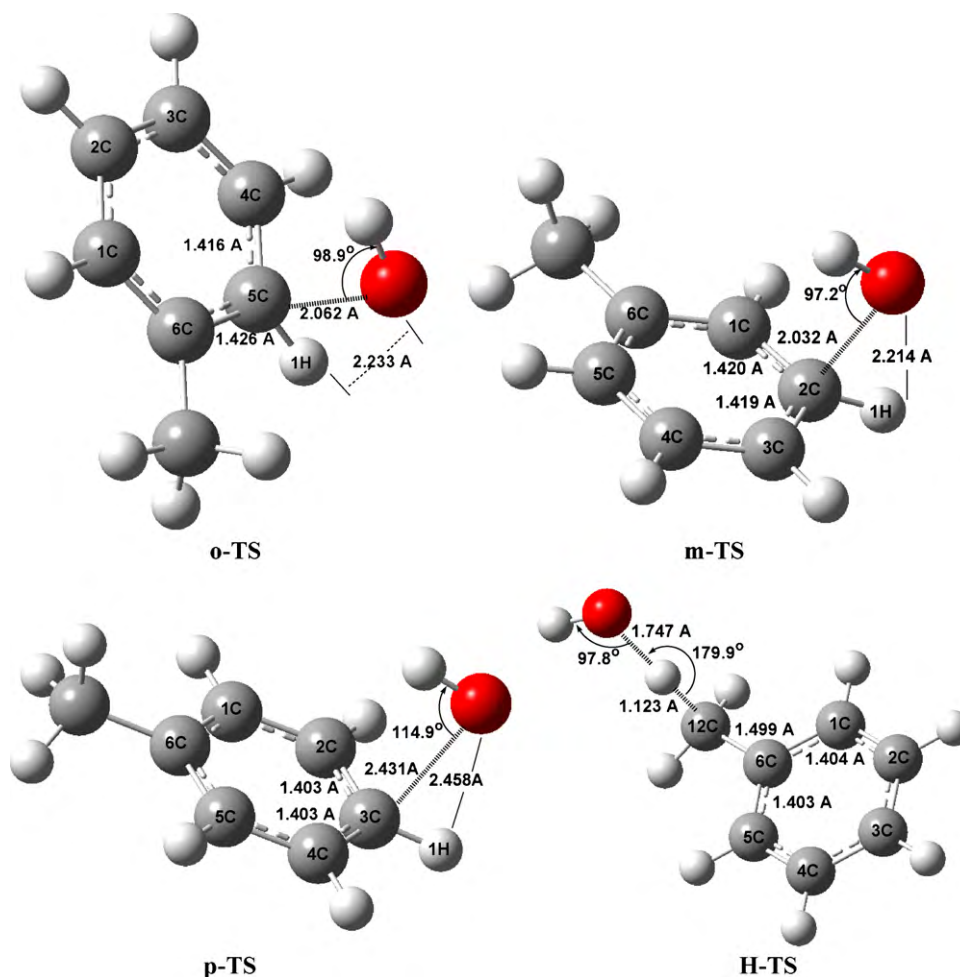


Fig. 4. The optimized structures of the transition state complexes.

$4.33 \times 10^{-13} \text{ cm}^3 \text{ molecule}^{-1} \text{ s}^{-1}$  reported by Knispel et al. [38]. By using the branching ratios, the relative concentrations of the primary intermediates were also calculated and are presented in Table 2. The results indicate that *ortho*-addition is the prevailing reaction path for both gas and aqueous phases, followed by *para*-addition in the gas phase and by *meta*-addition in the aqueous phase. Moreover, the calculated rate constants show that *ortho*-addition and H-abstraction proceed faster in the aqueous compared to the gas phase. In contrast, the rates of the remaining paths decrease in aqueous solution, coherently with the increase in the energy barriers due to the weakening effect of water molecules on the original hydrogen-bonds in the pre-reactive complexes.

The obtained product distribution indicates that the major primary intermediate of the photo-oxidative degradation of toluene is the *o*-R (1-hydroxy-2-methylcyclohexadienyl radical) which then forms *o*-cresol through abstraction of the redundant ring H by molecular oxygen. The reaction also yields *p*-R (1-hydroxy-4-methylcyclohexadienyl radical) and *m*-R (1-hydroxy-3-methylcyclohexadienyl radical), in lower amounts in water compared to the gas phase. The relative concentration of the benzyl radical that would then be converted to benzaldehyde through the reaction with  $\text{O}_2$  is much less than all the other reaction products. The formation of benzaldehyde could be more favored in solution compared to the gas phase, but the solvent effect is rel-

Table 2

Activation energies  $E_a$ , reaction energies  $E_r$ , rate constants and product distributions for the possible reaction paths.

	<i>o</i> -Addition	<i>m</i> -Addition	<i>p</i> -Addition	H-Abstraction
<i>Gas phase</i>				
$E_a$ (kcal mol <sup>-1</sup> )	0.38	0.41	0.01	1.07
$E_r$ (kcal mol <sup>-1</sup> )	-15.50	-13.73	-15.20	Endothermic
$k$ (cm <sup>3</sup> molecule <sup>-1</sup> s <sup>-1</sup> )	$7.61 \times 10^{-14}$	$3.43 \times 10^{-14}$	$9.80 \times 10^{-14}$	$3.11 \times 10^{-14}$
Branching ratio (%)	43.5	19.6	28.0	8.9
<i>Aqueous phase</i>				
$E_a$ (kcal mol <sup>-1</sup> )	0.26	0.54	0.50	1.01
$E_r$ (kcal mol <sup>-1</sup> )	-16.16	-13.61	-13.65	Endothermic
$k$ (cm <sup>3</sup> molecule <sup>-1</sup> s <sup>-1</sup> )	$9.34 \times 10^{-14}$	$2.74 \times 10^{-14}$	$4.31 \times 10^{-14}$	$3.41 \times 10^{-14}$
	$5.62 \times 10^{7a}$	$1.65 \times 10^7$	$2.59 \times 10^7$	$7.95 \times 10^6$
Branching ratio (%)	58.6	17.2	13.5	10.7

<sup>a</sup> The unit for the values in italic is  $\text{M}^{-1} \text{ s}^{-1}$ .



atively small and it is lower than the errors of the experimental data [8, and this work]. The computational results indicate that the products of the photo-oxidative degradation of toluene are *o*-cresol (*o*-CR), *p*-cresol (*p*-CR), *m*-cresol (*m*-CR) and benzaldehyde (B), with  $[o\text{-CR}] > [p\text{-CR}] > [m\text{-CR}] > [B]$  in the gas phase. The concentration order is  $[o\text{-CR}] > [m\text{-CR}] > [p\text{-CR}] > [B]$  in the aqueous phase, which is consistent with the experimental findings of this study.

#### 4.3. Environmental importance of toluene degradation

It is possible to foresee the half-life time of a water-dissolved compound CP because of reaction with  $\bullet\text{OH}$  ( $\tau_{\text{CP},\bullet\text{OH}}^{\text{SSD}}$ ), as a function of its second-order reaction rate constant with  $\bullet\text{OH}$ ,  $k_{\text{CP},\bullet\text{OH}}$ , the chemical composition of the surface water layer (and in particular the concentration values of the main sources and sinks of  $\bullet\text{OH}$ ), and the water column depth  $d$ . Note that  $d$  would be the average depth of thoroughly mixed water bodies or the mixing layer depth of large, stratified lakes. The half-life time units are summer sunny days (SSD), equivalent to a fair-weather 15 July at 45°N latitude. One gets  $\tau_{\text{CP},\bullet\text{OH}}^{\text{SSD}}$  as follows [21]:

$$\tau_{\text{CP},\bullet\text{OH}}^{\text{SSD}} = 1.9 \times 10^{-5} \frac{\sum_i k_{\text{Si}}[S_i]}{R_{\text{OH}}^{\text{tot}} k_{\text{CP},\bullet\text{OH}}} \quad (8)$$

where  $\sum_i k_{\text{Si}}[S_i]$  is the rate constant of the natural  $\bullet\text{OH}$  scavengers and  $R_{\text{OH}}^{\text{tot}}$  is the formation rate of  $\bullet\text{OH}$ , which depends on the concentration of the main  $\bullet\text{OH}$  sources (nitrate, nitrite and colored dissolved organic matter) and on the depth  $d$  of the water column. In the case of toluene it is  $k_{\text{CP},\bullet\text{OH}} = 3.0 \times 10^9 \text{ M}^{-1} \text{ s}^{-1}$  [39]. A more complete description of the adopted photochemical model is reported as Supplementary Material (hereafter SM).

Fig. 5(a) reports  $\tau_{\text{CP},\bullet\text{OH}}^{\text{SSD}}$  for toluene in the presence of 2.1 mM bicarbonate and 26  $\mu\text{M}$  carbonate, for  $d = 1 \text{ m}$  and different concentration values of the dissolved organic matter (expressed as NPOC, Non-Purgeable Organic Carbon) and nitrate/nitrite. Nitrate was set to vary in the range of 1–30  $\mu\text{M}$ , and it was hypothesized that  $[\text{NO}_3^-]/[\text{NO}_2^-] = 100$ . Such a concentration ratio is reasonable in surface waters [40,41]. The half-life time for reaction with  $\bullet\text{OH}$  is lower at higher nitrate and nitrite that are major  $\bullet\text{OH}$  sources (nitrite is also a very minor  $\bullet\text{OH}$  sink, but its role as scavenger is negligible compared to organic and inorganic carbon). Note the minimum of  $\tau_{\text{CP},\bullet\text{OH}}^{\text{SSD}}$  for NPOC  $\sim 1 \text{ mg CL}^{-1}$  in the presence of low nitrate and nitrite. The reason for the minimum is that, under such conditions, colored dissolved organic matter (CDOM) could prevail over nitrate/nitrite as  $\bullet\text{OH}$  source and, at the same time, carbonate and bicarbonate would scavenge  $\bullet\text{OH}$  to a comparable extent as organic matter itself. Therefore, for NPOC  $< 1 \text{ mg CL}^{-1}$ , the production of  $\bullet\text{OH}$  by dissolved organic compounds would prevail over the scavenging. At elevated NPOC, the general increase of the half-life times is accounted for by the combination of  $\bullet\text{OH}$  scavenging and radiation screening that are carried out by dissolved organic matter. Fig. 5(a) also reports the time interval that is hypothesized for the biological degradation of toluene in surface waters (1–6 months; [16]). It can be observed that the lifetime with  $\bullet\text{OH}$  can be comparable to or even lower than that for the biological degradation, provided that nitrate and nitrite are present in sufficiently high concentration and that NPOC is not too high.

Fig. 5(b) reports the expected time trends of 10 nM toluene ( $\sim 1 \mu\text{g L}^{-1}$ ), cresols and benzaldehyde in the presence of 30  $\mu\text{M}$  nitrate, 0.3  $\mu\text{M}$  nitrite, 1  $\text{mg CL}^{-1}$  NPOC, 2.1 mM bicarbonate and 26  $\mu\text{M}$  carbonate, for  $d = 1 \text{ m}$ , under the hypothesis that all the compounds are formed and transformed upon reaction with  $\bullet\text{OH}$  (the formation yields of the intermediates as reported in Table 1 were considered). The reaction rate constants with  $\bullet\text{OH}$  of *o*-cresol, *p*-cresol and benzaldehyde are  $1.1 \times 10^{10}$ ,  $1.2 \times 10^{10}$  and

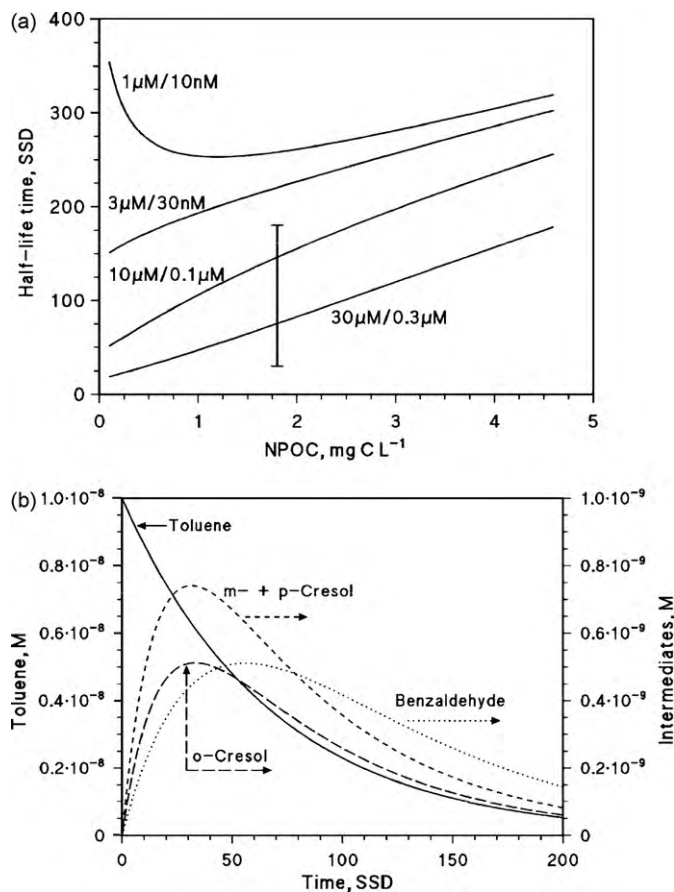


**Fig. 5.** (a) Half-life time of toluene in the presence of 2.1 mM bicarbonate and 26  $\mu\text{M}$  carbonate, for  $d = 1 \text{ m}$ , as a function of  $[\text{NO}_3^-]/[\text{NO}_2^-] = 100$  and of the NPOC. The vertical line represents the estimated lifetime for biological degradation (1 to 6 months [16]). (b) Time trend of toluene and of its main transformation intermediates upon reaction with  $\bullet\text{OH}$ , in the presence of 30  $\mu\text{M}$  nitrate, 0.3  $\mu\text{M}$  nitrite, 1  $\text{mg CL}^{-1}$  NPOC, 2.1 mM bicarbonate and 26  $\mu\text{M}$  carbonate, for  $d = 1 \text{ m}$ , under the hypothesis that all the compounds undergo transformation with  $\bullet\text{OH}$  alone. The time evolution curve of toluene is plotted against the left-hand Y-axis, while those of the intermediates (cresols and benzaldehyde) are plotted against the right-hand Y-axis (note the different scales). The arrows point toward the axis relevant to each curve.

$4.4 \times 10^9 \text{ M}^{-1} \text{ s}^{-1}$ , respectively [39]. The reaction rate constant of *m*-cresol is not reported but, given the similar values for the other two isomers, a reasonable approximation is to use the literature rate constant of *p*-cresol. Interestingly, all the transformation intermediates would be more reactive than toluene toward  $\bullet\text{OH}$ . By application of the model equation (8) and considering that  $k_{\text{CP}}^d = 0.693 (\tau_{\text{CP},\bullet\text{OH}}^d)^{-1}$ , under the hypothesized conditions it is  $\tau_{\text{tol},\bullet\text{OH}} = 47 \text{ SSD}$  ( $k_{\text{tol}}^d = 1.5 \times 10^{-2} \text{ SSD}^{-1}$ ),  $\tau_{o\text{-cr},\bullet\text{OH}} = 13 \text{ SSD}$  ( $k_{o\text{-cr}}^d = 5.4 \times 10^{-2} \text{ SSD}^{-1}$ ),  $\tau_{m\text{-cr},\bullet\text{OH}} = \tau_{p\text{-cr},\bullet\text{OH}} = 12 \text{ SSD}$  ( $k_{m/p\text{-cr}}^d = 5.9 \times 10^{-2} \text{ SSD}^{-1}$ ), and  $\tau_{\text{benzald},\bullet\text{OH}} = 32 \text{ SSD}$  ( $k_{\text{benzald}}^d = 2.2 \times 10^{-2} \text{ SSD}^{-1}$ ). The time trend of toluene in Fig. 5(b) was plotted with Eq. (1), that of the intermediates with Eq. (2). It can be seen that the concentrations of the intermediates would reach a maximum in approximately 50 SSD, and that the sum of their concentrations would never exceed 20% of the initial toluene. Note that benzaldehyde is the intermediate formed in lower yield but it is the most stable toward  $\bullet\text{OH}$ . The outcome is that benzaldehyde would be the most concentrated intermediate at long transformation times. Also note that the cresols could be transformed faster than foreseen by the adopted model, because they also undergo important reactions with the excited triplet states of CDOM [42].



## 5. Conclusions

Hydroxyl radicals, photogenerated by UVB irradiation of nitrate oxidize toluene by pseudo-first-order reaction rates. The experimental findings indicate that  $\bullet\text{OH}$  mainly attacks the aromatic ring of toluene to produce the cresols (hydroxymethylbenzenes) with a total yield of  $(78 \pm 16)\%$ , and benzaldehyde through the abstraction of a hydrogen atom from the methyl group, with a yield of about  $(17 \pm 3)\%$ . Based on the quantum mechanical calculations, four different reaction paths have been determined for the reaction of toluene with  $\bullet\text{OH}$ . DFT calculations indicate the formation of pre-reactive complexes between the  $\bullet\text{OH}$  radical and toluene as the precursors to the reaction. The addition complexes are early transition states, whereas the abstraction complex is formed late along the reaction coordinate. The activation energies for the addition paths are lower than that for the abstraction path due to hydrogen-bonding. The presence of a dielectric continuum such as water increases the stability of all the species but it also alters the energy barriers. In both the gas and aqueous phases, the  $\bullet\text{OH}$  attack on the ring prevails over that on the methyl group. Based on aqueous photochemistry modeling, it is suggested that the  $\bullet\text{OH}$  reaction could be a competitive sink for toluene in surface waters compared to microbial processes, in nitrate/nitrite-rich and DOM-poor water bodies.

Interestingly, the  $\bullet\text{OH}$  radical has been found to undergo accumulation at the air–water interfaces compared to the solution bulk [43]. Also toluene could be accumulated at the interface, in a similar way as benzene [44], and the combination of the two phenomena could greatly enhance the interface reaction compared to the bulk. The overall effect would hardly be significant in surface water bodies where the interface is a negligible fraction of the total volume. However, it could be important in atmospheric droplets that have radii in the micrometer range and, therefore, possess a very favorable surface-to-volume ratio [44,45].

## Acknowledgements

The authors express their thanks to Yıldız Technical University Research Foundation (Project No: 24-01-02-15), PNRA-Progetto Antartide and MIUR-PRIN 2007 (2007L8Y4NB, Area 02, Project No: 36) for financial support.

## Appendix A. Supplementary data

Supplementary data associated with this article can be found, in the online version, at doi:10.1016/j.jphotochem.2010.07.021.

## References

- [1] B.J. Finlayson-Pitts, J.N. Pitts Jr., Chemistry of the Upper and Lower Atmosphere, Academic Press, San Diego, 2000.
- [2] B. Bohn, Formation of peroxy radicals from OH–toluene adducts and  $\text{O}_2$ , J. Phys. Chem. 105 (2001) 6092–6101.
- [3] I. Suh, D. Zhang, R. Zhang, L.T. Molina, M.J. Molina, Theoretical study of OH addition reaction to toluene, Chem. Phys. Lett. 364 (2002) 454–462.
- [4] T. Seto, M. Nakajima, A. Miyoshi, High-temperature reactions of OH radicals with benzene and toluene, J. Phys. Chem. A 110 (2006) 5081–5090.
- [5] M. Bekbolet, Z. Çınar, M. Kılıç, C.S. Uyguner, C. Minero, E. Pelizzetti, Photocatalytic oxidation of dinitronaphthalenes: theory and experiment, Chemosphere 75–8 (2009) 1008–1014.
- [6] P. Bruno, M. Caselli, G. De Gennaro, L. Scolletta, L. Trizio, M. Tutino, Assessment of the impact produced by traffic source on VOC level in the urban area of Canosa di Puglia (Italy), Water Air Soil Pollut. 193 (2008) 37–50.
- [7] R.N. Wixtrom, S.L. Brown, Individual and population exposures to gasoline, J. Expo. Anal. Environ. Epidemiol. 2 (1992) 23–78.
- [8] R. Atkinson, Gas-phase tropospheric chemistry of organic compounds, in: J.W. Gallagher (Ed.), J. Phys. Chem. Ref. Data, Monograph n. 2, 1994.
- [9] P.T. Katsumata, W.E. Kastenberg, Fate and transport of methanol fuel from spills and leaks, Hazard. Waste Hazard. Mater. 13 (1996) 495–498.
- [10] D. Holdway, D.T. Heggie, Direct hydrocarbon detection of produced formation water discharge on the Northwest Shelf, Australia, Estuar. Coast. Shelf Sci. 50 (2000) 387–402.
- [11] I. Arambarri, M. Lasa, R. Garcia, E. Millan, Determination of fuel dialkyl ethers and BTEX in water using headspace solid-phase microextraction and gas chromatography-flame ionization detection, J. Chromatogr. A 1033 (2004) 193–203.
- [12] B. Karacanjic, L. Skender, V. Karacic, Benzene, toluene, ethylbenzene, and isomeric xylenes in various water samples in Canada, Bull. Environ. Contam. Toxicol. 76 (2006) 458–463.
- [13] S.C. Soh, M.P. Abdullah, Determination of volatile organic compounds pollution sources in Malaysian drinking water using multivariate analysis, Environ. Monit. Assess. 124 (2007) 39–50.
- [14] D. Fatta, C. Michael, S. Canna-Michaelidou, M. Christoulidou, N. Kythreotou, M. Vasquez, Pesticides, volatile and semivolatile organic compounds in the inland surface waters of Cyprus, Desalination 215 (2007) 223–236.
- [15] C. Robinson, A. Brovelli, D.A. Barry, L. Li, Tidal influence on BTEX biodegradation in sandy coastal aquifers, Adv. Water Resour. 32 (2009) 16–28.
- [16] P.C. Heald, S.G. Schladow, J.E. Reuter, B.C. Allen, Modeling MTBE and BTEX in lakes and reservoirs used for recreational boating, Environ. Sci. Technol. 39 (2005) 1111–1118.
- [17] J. Hoigné, Formulation and calibration of environmental reaction kinetics: oxidations by aqueous photooxidants as an example, in: W. Stumm (Ed.), Aquatic Chemical Kinetics, John Wiley and Sons, New York, 1990, pp. 43–70, Chapter 2.
- [18] P.L. Brezonik, J. Fulkerson-Brekken, Nitrate-induced photolysis in natural waters: controls on concentrations of hydroxyl radical photo-intermediates by natural scavenging agents, Environ. Sci. Technol. 32 (1998) 3004–3010.
- [19] V.H. Uc, I.G. Cruz, A.H. Laguna, A.V. Bunge, New channels in the reaction mechanism of the atmospheric oxidation of toluene, J. Phys. Chem. A 104 (2000) 7847–7855.
- [20] D. Vione, S. Khanra, S. Cucu Man, P.R. Maddigapu, R. Das, C. Arsene, R.I. Olariu, V. Maurino, C. Minero, Inhibition vs. enhancement of the nitrate-induced phototransformation of organic substrates by the  $\bullet\text{OH}$  scavengers bicarbonate and carbonate, Water Res. 43 (2009) 4718–4728.
- [21] D. Vione, R. Das, F. Rubertelli, V. Maurino, C. Minero, S. Barbati, S. Chiron, Modelling the occurrence and reactivity of hydroxyl radicals in surface waters: implications for the fate of selected pesticides, Int. J. Environ. Anal. Chem. 90 (2010) 258–273.
- [22] J.H. Kuhn, S.E. Braslavsky, R. Schmidt, Chemical actinometry, Pure Appl. Chem. 76 (2004) 2105–2146.
- [23] J. Mack, J.R. Bolton, Photochemistry of nitrite and nitrate in aqueous solution: a review, J. Photochem. Photobiol. A: Chem. 128 (1999) 1–13.
- [24] M.J. Frisch, G.W. Trucks, H.B. Schlegel, G.E. Scuseria, M.A. Robb, J.R. Cheeseman, J.A. Montgomery Jr., T. Vreven, K.N. Kudin, J.C. Burant, J.M. Millam, S.S. Iyengar, J. Tomasi, V. Barone, B. Mennucci, M. Cossi, G. Scalmani, N. Rega, G.A. Petersson, H. Nakatsuji, M. Hada, M. Ehara, K. Toyota, R. Fukuda, J. Hasegawa, M. Ishida, T. Nakajima, Y. Honda, O. Kitao, H. Nakai, M. Klene, X. Li, J.E. Knox, H.P. Hratchian, J.B. Cross, C. Adamo, J. Jaramillo, R. Gomperts, R.E. Stratmann, O. Yazyev, A.J. Austin, R. Cammi, C. Pomelli, J.W. Ochterski, P.Y. Ayala, K. Morokuma, G.A. Voth, P. Salvador, J.J. Dannenberg, V.G. Zakrzewski, S. Dapprich, A.D. Daniels, M.C. Strain, O. Farkas, D.K. Malick, A.D. Rabuck, K. Raghavachari, J.B. Foresman, J.V. Ortiz, Q. Cui, A.G. Baboul, S. Clifford, J. Cioslowski, B.B. Stefanov, G. Liu, A. Liashenko, P. Piskorz, I. Komaromi, R.L. Martin, D.J. Fox, T. Keith, M.A. Al-Laham, C.Y. Peng, A. Nanayakkara, M. Challacombe, P.M.W. Gill, B. Johnson, W. Chen, M.W. Wong, C. Gonzalez, J.A. Pople, Gaussian 03, Revision B.04, Gaussian, Inc., Pittsburgh, PA, 2003.
- [25] M.W. Wong, L. Radom, Radical additions to alkenes: further assessment of the theoretical procedures, J. Phys. Chem. A 102 (1998) 2237–2245.
- [26] A.S. Ozen, V. Aviyente, R.A. Klein, Modeling the oxidative degradation of azo dyes: a density functional theory study, J. Phys. Chem. A 107 (2003) 4898–4907.
- [27] J. Andzelm, C. Kölmel, A. Klamt, Incorporation of solvent effects into density-functional calculations of molecular-energies and geometries, J. Chem. Phys. 103 (1995) 9312–9320.
- [28] V. Barone, M. Cossi, Quantum calculation of molecular energies and energy gradients in solution by a conductor solvent model, J. Phys. Chem. A 102–11 (1998) 1995–2001.
- [29] J.B. Foresman, M. Frisch, Exploring Chemistry with Electronic Structure Methods, Gaussian Inc., Pittsburgh, PA, 1996.
- [30] N.S. Hush, J. Schamberger, G.B. Bacskay, A quantum chemical computational study of the relative stabilities of cis- and transplatinum dichloride in aqueous solution, Coord. Chem. Rev. 249 (2005) 299–311.
- [31] X.Q. Wang, J.P. Wu, M.W. Zhao, Y.F. Lv, G.Y. Li, C.W. Hu, Partial oxidation of toluene in  $\text{CH}_3\text{COOH}$  by  $\text{H}_2\text{O}_2$  in the presence of  $\text{VO}(\text{acac})_2$  catalyst, J. Phys. Chem. C 113 (2009) 14270–14278.
- [32] V. Brezová, M. Ceppan, E. Brandsteterova, M. Breza, L. Lapcik, Photocatalytic hydroxylation of benzoic acid in aqueous titanium dioxide suspension, J. Photochem. Photobiol. A: Chem. 59 (3) (1991) 385–391.
- [33] M. Kılıç, G. Koçturk, N. San, Z. Çınar, A model for product distributions for the reactions of phenol derivatives with hydroxyl radicals, Chemosphere 69 (9) (2007) 1396–1408.
- [34] F.P. Tully, A.R. Ravishankara, R.L. Thompson, J.M. Nicovich, R.C. Shah, N.M. Kreutter, P.H. Wine, Kinetics of the reactions of hydroxyl radical with benzene and toluene, J. Phys. Chem. 85 (1981) 2262–2269.
- [35] V.H. Uc, J.R. Alvarez-Idaboy, A. Galano, I.G. Cruz, A.V. Bunge, Theoretical determination of the rate constant for oh hydrogen abstraction from toluene, J. Phys. Chem. A 110 (2006) 10155–10162.

- [36] M.K. Eberhardt, M. Yoshida, Radiation-induced homolytic aromatic substitution. I. Hydroxylation of nitrobenzene, chlorobenzene, and toluene, *J. Phys. Chem.* 77-5 (1973) 589–597.
- [37] W.J. Hehre, L. Radom, P.R. Schleyer, J.A. Pople, *Ab initio Molecular Orbital Theory*, Wiley, New York, 1986.
- [38] R. Knispel, R. Koch, M. Siese, C. Zetzsch, Adduct formation of OH radicals with benzene, toluene and phenol and consecutive reactions of the adducts with NO<sub>x</sub> and O<sub>2</sub>, *Ber. Bunsenges. Phys. Chem.* 94 (1990) 1375–1379.
- [39] G.V. Buxton, C.L. Greenstock, W.P. Helman, A.B. Ross, Critical review of rate constants for reactions of hydrated electrons, hydrogen atoms and hydroxyl radicals ( $\cdot\text{OH}/\cdot\text{O}^-$ ) in aqueous solution, *J. Phys. Chem. Ref. Data* 17 (1988) 1027–1284.
- [40] K. Takeda, H. Takedoi, S. Yamaji, K. Ohta, H. Sakugawa, Determination of hydroxyl radical photoproduction rates in natural waters, *Anal. Sci.* 20 (2004) 153–158.
- [41] C. Minero, S. Chiron, G. Falletti, V. Maurino, E. Pelizzetti, R. Ajassa, M.E. Carlotti, D. Vione, Photochemical processes involving nitrite in surface water samples, *Aquat. Sci.* 69 (2007) 71–85.
- [42] S. Canonica, M. Freiburghaus, Electron-rich phenols for probing the photochemical reactivity of freshwaters, *Environ. Sci. Technol.* 35 (2001) 690–695.
- [43] M. Roeselova, J. Vieceli, L.X. Dang, B.C. Garrett, D.J. Tobias, Hydroxyl radical at the air–water interface, *J. Am. Chem. Soc.* 126 (2004) 16308–16309.
- [44] D. Vione, C. Minero, A. Hamraoui, M. Privat, Modelling photochemical reactions in atmospheric water droplets: an assessment of the importance of surface processes, *Atmos. Environ.* 41 (2007) 3303–3314.
- [45] P. Nissenon, C.J.H. Knox, B.J. Finlayson-Pitts, L.F. Phillips, D. Dabdub, Enhanced photolysis in aerosols: evidence for important surface effects, *Phys. Chem. Chem. Phys.* 8 (2004) 4700–4710.